A Photographic Study of Pool Boiling in the Region of the Critical Heat Flux

ROBERT COLE

Lewis Research Center, National Aeronautics and Space Administration, Cleveland, Ohio

A photographic study was made to investigate the boiling phenomena in the neighborhood of the critical heat flux. The system consisted of an electrically heated zirconium ribbon, insulated on its underface, suspended in a pool of water at its saturation temperature. Measurements of bubble diameters, bubble positions relative to the heating surface, local bubble frequencies, and contact angles at known times intervals were obtained from the film. Results indicate that at high heat fluxes the primary forces acting on a bubble leaving the surface are the buoyancy and drag forces. A dimensionless relationship is developed relating bubble velocity, bubble diameter, and contact angle at breakoff. Drag coefficients for freely rising vapor bubbles in saturated liquid are found to be representable by the usual drag coefficient-Reynolds number curves for solid bodies. Jakob's plot of bubble frequency vs. bubble diameter at breakoff is extended to high heat-flux values, and a relationship proposed by Deissler at the critical heat flux is found to yield reasonable agreement with the experimental data.

The use of boiling fluids as an efficient means of cooling such high heat flux devices as nuclear reactors and rocket engines is of interest owing to the relatively high heat transfer rates made possible by the boiling process. The physical nature of this process is such that it must be classified into three separate and distinct regimes; nucleate, transitional, and film boiling. Nucleate is characterized by the emination of bubbles from certain discrete positions on the heating surface. Increasing heat flux results in an increase in both the surface temperature and bubble population. At higher fluxes the bubble population increases to such an extent that the bubbles coalesce and the surface becomes completely covered with a highly unstable irregular film of vapor. This hydrodynamic event marks the end of the nucleate boiling region and the beginning of the transitional region. The mechanism which yielded high heat transfer rates in the nucleate region is nonexistent in the transitional, and as a result, if the power level in the system is maintained, the surface temperature must increase. Eventually the film becomes stable, intermittently shooting off large bubbles at regularly spaced intervals along the surface. Stable operation is possible in this region provided that the combined effects of conduction and radiation yield a heat transfer rate equal to the power level prior to failure of the heating surface by melting. In many instances when the power level is being controlled (rather than the surface temperature), the material will melt locally either during the transition region or the film boiling region prior to the attainment of stable operation. Such an occurrence is commonly called *burnout* and results in the destruction of the device. In order to design against burnout and yet obtain high heat transfer rates it is necessary that some means be available for predicting the heat flux at which coalescence of the vapor bubbles occurs (the critical heat flux).

Rohsenow and Griffith (*12*) successfully correlated critical heat flux data for saturated liquids by the relationship

$$\frac{q_c}{\lambda_v \rho_v} = C_1 \left[\frac{\rho_l - \rho_v}{\rho_r} \right]^n \qquad (1)$$

where C_1 and n are experimentally determined constants having the values 14.3 ft./hr. and 0.6, respectively. The group on the left is a superficial vapor velocity and is obtained by assuming a close-packed arrangement of vapor bubbles on the heating surface such that all of the generated heat is dissipated as latent heat. The density ratio on the right may be considered as a buoyancy force per unit mass of vapor, and it is assumed that the superficial vapor velocity is proportional to some power of the buoyancy force.

Forster and Zuber (*4*) have obtained expressions for the growth of a spherical vapor bubble completely surrounded by a superheated liquid. Finding that the product of the bubble radius and radial velocity were independent of time one could formulate a bubble Reynolds number and correlate critical heat flux data by the familiar relationship

$$N_{Nu} = C_2 N^{n_1}_{Re} N^{m}_{Pr} \qquad (2)$$

Unfortunately the Nusselt number, which contains the critical heat flux, also contains the critical temperature difference which is not generally known.

Kutateladze (*9*), assuming the occurrence of the critical heat flux to be due to hydrodynamic effect alone, utilizes the equation of motion and energy equation to obtain the following relationship by dimensional analysis:

$$\frac{q_c}{\lambda_v \rho_v^{1/2} [\sigma_{lv} g (\rho_l - \rho_v)]^{1/4}} = K = \text{const.} \qquad (3)$$

Sterman (*14*) utilizing the equation for convective heat transfer with a heat source, an equation describing the transfer of heat due to boiling from the laminar-transition layers to the turbulent core and the dimensionless groups resulting from the equation of motion, obtains, also by means of dimensional analysis, an expression identical to Equation (3).

Deissler (*2*) employing a physical model of the boiling mechanism at the critical heat flux obtains a relationship similar to Equation (3) without resorting to dimensional analysis. It is postulated that the critical heat flux occurs when the rate of formation of bubbles just exceeds the rate at which they are carried away. Under these conditions the drag on the bubbles is sufficient for successive bubbles leaving the surface to touch and coalesce. When one utilizes the relationship obtained by Fritz (*5*) between bubble diameter and contact angle at breakoff, an expression for the rate at which bubbles are carried away, and an expression for the heat flux identical to that employed by Rohsenow and Griffith, the relationship

$$\frac{q_c}{\lambda_v \rho_v^{1/2} [\sigma_{lv} g (\rho_l - \rho_v)]^{1/4}} = C_3 \frac{\beta^{1/2}}{C_D^{1/2}} \qquad (4)$$

is obtained. If the drag coefficient and contact angle at breakoff are assumed constant, Equation (4) is identical to Equation (3).

Zuber (*17*) in a stability analysis of the boiling mechanism on the transitional side of the critical heat flux ob-

Robert Cole is at Clarkson College of Technology, Potsdam, New York.

tains the following theoretical relationship:

$$\frac{q_c}{\lambda_v \rho_v^{1/2}[\sigma_{lv} g(\rho_l - \rho_v)]^{1/4}} = \frac{\pi}{24}\left(\frac{\rho_l + \rho_v}{\rho_l}\right) \qquad (5)$$

It is shown by Zuber and Tribus (*18*) that the constant $\pi/24$ is actually an average value having the theoretical limits 0.157 to 0.12. Except for the last group on the right, which under most conditions will have a numerical value of unity, Equation (5) is also identical to Equation (3). The constant $\pi/24$ should thus agree with the value of K obtained employing experimental data. Kutateladze obtained $K = 0.16$ and Sterman 0.168.

Borishanskii (*1*), extending Kutateladze's analysis to include the effects of viscosity, obtained the relationships

$$K = 0.13 + 4N^{-0.4} \qquad (6)$$

or

$$K = 0.8\,N^{-1/8} \qquad (7)$$

where

$$N = \frac{\rho_l \sigma_{lv}^{3/2}}{\mu_l^2[g(\rho_l - \rho_v)]^{1/2}} \qquad (8)$$

Deissler (*2*) obtained a functional relationship between K and a bubble Reynolds number which except for the use of vapor properties is equal to $N^{1/2}$. This relationship follows directly from Equation (4) by assuming the contact angle, which is dependent upon surface conditions, to be constant and by assuming the drag coefficient to be some function of a bubble Reynolds number. Modification of the Reynolds number by substituting expressions for the bubble velocity and diameter yields the relationship

$$K = f_1\left\{\frac{\rho_v^{1/2}\sigma_{lv}^{3/4}}{\mu_v[g(\rho_l - \rho_v)]^{1/4}}\right\} \qquad (9)$$

where K has replaced the group on the left-hand side of Equation (3). No significant trend of K with the group in brackets was found, or in other words the drag coefficient was found to be independent of Reynolds number. The relationship obtained was $K = 0.15$.

It would seem, from the success of the various models, that the dynamics of the boiling mechanism in the neighborhood of the critical heat flux would be well known. Zuber's analysis, which approaches the problem from the standpoint of the breakdown of transitional boiling, sheds little light on the bubble mechanism on the nucleate side of the critical heat flux. Both Kutateladze and Sterman found it necessary to employ dimensional analysis techniques, while Deissler, using possibly the most appealing approach, was required to make experimentally unverified assumptions as to the dynamics of his model. The purpose of this paper is to give an insight into the dynamics of the boiling mechanism in the neighborhood of the critical heat flux.

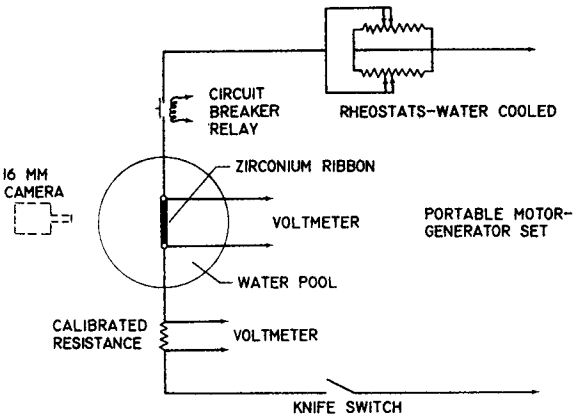

Fig. 1. Schematic diagram of apparatus.

APPARATUS

The system is illustrated schematically in Figure 1. It consisted of a zirconium ribbon suspended horizontally by means of two copper rods in a pool of boiled-distilled water, a calibrated resistance, two 4,000-W. water cooled rheostats connected in parallel, and a portable motor generator set. The zirconium ribbon, which was 3 x 3/16 x 0.006 in., was insulated on its underface by a glyptal coating and was heated electrically by means of direct current originating in the motor-generator set. The container itself was a 2-liter Pyrex beaker wrapped with asbestos cloth insulation to minimize heat losses. The insulation was removed on opposite sides of the vessel from just below the level of the ribbon up to the surface level of the water so that the boiling mechanism could be observed. The power input to the ribbon was measured by means of a voltmeter attached across the copper rods and a second voltmeter attached across the calibrated resistance. The boiling action on the ribbon was recorded by means of a 16-mm. camera, equipped with a 50 mm. f/2 lens, operating at a rate of 5,000 f./sec. Lighting was provided by means of three lamps located above and behind the pool. One thousand cycle per second timing marks were recorded on the film by means of a calibrated oscillator, an amplifier, and an argon timing lamp within the camera. No means were provided for the determination of transient surface temperatures or heat-flux densities.

EXPERIMENTAL PROCEDURE

The power input to the zirconium ribbon was initially set at a level well below that corresponding to the critical heat flux and was maintained at that level until the entire mass of water had reached its saturation temperature. The power was then increased until it was just below the level at which it was known that instability and burnout would occur and maintained at this value for a period of 5 min. Owing to the essentially negligible resistance of the ribbon compared with the total resistance of the circuit, any sudden increase in ribbon resistance due to an increase in the average ribbon temperature, while the power level was being raised, resulted in an abnormally rapid increase in voltage drop across the ribbon. The abnormal rise in voltage drop was used as an indication of the moment to start the camera, which was operated by means of a push button located on the panel board. It was estimated that the total elapsed time between the moment the abnormal increase in voltage was first noticeable, and the moment that burnout occurred was 2 sec. As the voltage increase seemed to be of an exponential nature, it was found possible to cut the power input at almost any time during the voltage rise and prevent burnout from occurring. With this procedure three overlapping runs were made, each exposing 100 ft. of film at 5,000 f./sec. The first run covered the period from the time at which the power input was increased from its set stable value up to the moment of the abnormal voltage rise. The second exposure was triggered at the moment the voltage began its abnormal rise and was completed and the power cut just prior to burnout. The third exposure of 100 ft. was initiated approximately 1 sec. after the voltage had begun to increase rapidly and was concluded after burnout had occurred. A fourth run was included with a second ribbon used, in which simultaneously the power input was increased to a very high level and the recording action begun. This exposure covered the boiling action from just below the critical heat flux up to ribbon burnout. A loan copy of the film, together with motion pictures of the apparatus and its operation, are available on request from the National Aeronautics and Space Administration, Lewis Research Center, Cleveland, Ohio.

METHODS OF MEASUREMENT AND CALCULATION

In order to obtain quantitative information on the dynamics of the boiling mechanism the original negatives were examined on a viewer with a magnification of 11:1, such that the

projected images were approximately twice their actual size. Frame-by-frame tracings were made of the bubbles and the time lapse between successive tracings obtained from timing marks on the film. A known vertical distance appeared in each frame, so that vertical distances on the tracings could be scaled to actual size. In obtaining measurements of bubble size the horizontal distances involved were small relative to the diameter of the container, so that errors due to distortion were negligible. Because the bubbles, in general, were not spherical, and because the field of view was two dimensional, it was assumed for the purpose of calculating bubble volumes that the bubbles were ellipsoidal with semiaxes $b = c \neq a$, the a axis being parallel to the ribbon length. The bubble volume is given by

$$V_b = \frac{4}{3}\pi abc \qquad (10)$$

and the surface area of the bubble by

$$S_b = 2\pi ac\left[\frac{\sin^{-1}\epsilon}{\epsilon} + (1-\epsilon^2)^{1/2}\right] \qquad (11)$$

where

$$\epsilon = \frac{(a^2-c^2)^{1/2}}{a}$$

The bubble diameters referred to throughout the paper are defined as the diameter of a sphere having the same volume as a bubble:

$$D_s = \left[\frac{6}{\pi}V_b\right]^{1/3} \qquad (12)$$

Freely rising bubbles

Frame-by-frame tracings were made of freely rising vapor bubbles. The position of the ribbon was included in each tracing so that the vertical distance the bubble had traveled was known for each time interval. Figure 2 shows a typical plot of distance traveled vs. time. (The conversion factor is 2.6 x 10^{-3} ft./unit.) The bubble

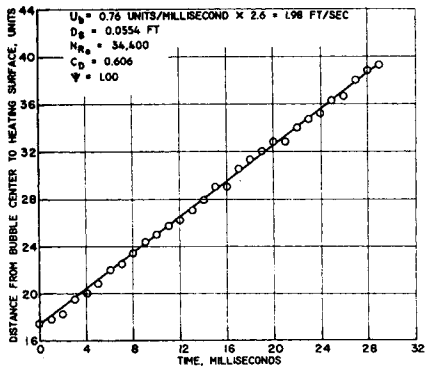

Fig. 2. Distance of a freely rising vapor bubble (maximum height) from heating surface as a function of time. The time at which the bubble distance and size were first determined was taken as time zero.

velocity was obtained from the slope of the curve. Maximum horizontal and vertical bubble dimensions were tabulated for each tracing and arithmetic averages used to obtain the bubble volumes from Equation (10). The bubble diameters were then obtained from Equation (12). Drag coefficients and Reynolds numbers were calculated for each freely rising vapor bubble. The drag coefficient is defined by the relationship

$$C_D = \frac{4g(\rho_l - \rho_v)D_s}{3\rho_l u_b^2} \qquad (13)$$

obtained by equating the buoyancy force acting on a freely rising bubble to the drag force. The bubble Reynolds number is given by

$$N_{Re} = \frac{D_s u_b \rho_l}{\mu_l} \qquad (14)$$

A measure of the deviation of the shape of a bubble from that of a sphere is given by the sphericity, defined as the surface area of a sphere having the same volume as the bubble, divided by the surface area of the bubble:

$$\psi = \frac{\pi\left(\frac{6V_b}{\pi}\right)^{2/3}}{S_b} = \frac{\pi D_s^2}{S_b} \qquad (15)$$

Vapor bubbles growing from a heated surface

At high heat-flux values frame-by-frame examination of the boiling action indicates that in the initial stage of bubble growth very small vapor bubbles coalesce on the heating surface to form patches of vapor. The patches of vapor, once formed, grow as single bubbles, eventually detach from the surface, and then rise through the surrounding saturated liquid. At the critical heat flux, and in the transition region, it appears that the entire surface may be covered with vapor. The vapor patches themselves have coalesced, and no solid-liquid contact exists. In this work bubbles were examined from both the nucleate and transitional side of the critical heat flux. Thus some of the bubbles were detaching from the heating surface and some from an irregular film of vapor. No distinction was made between the two.

Frame-by-frame tracings were made of vapor bubbles growing from the ribbon surface. A plot of the distance between the ribbon and the maximum height of the vapor bubble vs. time is shown in Figure 3. (The conversion factor is 2.6 x 10^{-3} ft./unit.) In most cases the curve became linear well before the bubble broke away from the surface. The slope of the linear portion of this curve was taken as the bubble velocity at breakoff; also recorded was the contact angle at breakoff. When the vapor film did exist, its thickness was small in comparison with the diameter of a departing bubble. As a result the contact angle was determined as if no vapor film existed and was measured just prior to the necking down of the bubble.

The local frequency of bubble formation was determined by recording the time lapse between the moment a bubble broke from the ribbon at a specific location and the moment the next bubble growing at the same location broke from the surface. A tracing was made of the second bubble and its diameter determined.

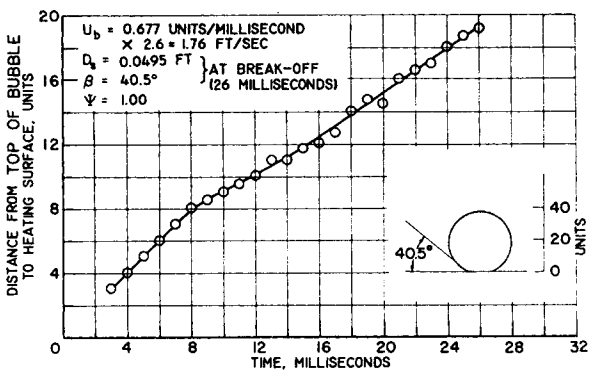

Fig. 3. Distance of an attached vapor bubble from heating surface as a function of time. The time at which the bubble first became noticeable was taken as time zero.

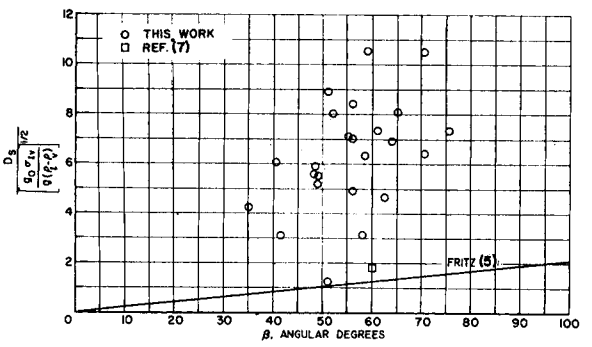

Fig. 4. Comparison of the correlation of Fritz (6) with data obtained at high heat fluxes.

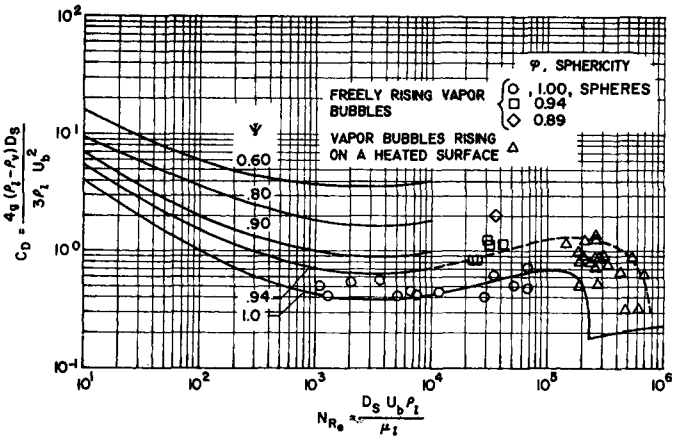

Fig. 5. Drag coefficient vs. Reynolds number for steam bubbles rising in water at its normal saturation temperature.

RESULTS AND DISCUSSION

Two aspects of the boiling mechanism were considered in this work: the motion of the vapor bubbles while attached to the surface, and the motion of the vapor bubbles after having left the surface. The problem of the growth of spherical vapor bubbles surrounded by superheated liquid has been treated by Forster and Zuber (*3*) and Plesset and Zwick (*11*). Comparison of their results with vapor bubbles growing on solid surfaces (Ellion's data) yields apparent agreement (*15*). Griffith (*6*) has recently considered the problem of the growth of a hemispherical bubble from a surface over a range of conditions. In addition to the rate of growth of a vapor bubble it is also of interest to be able to predict the diameter of a bubble at the moment it leaves the heating surface. Such an event occurs when the liquid is at its saturation temperature. It is noted from Figure 3 that the bubble velocity becomes approximately constant at some time prior to its leaving the surface. When one equates the buoyancy force acting on a bubble just prior to breakoff to the surface-tension forces acting on the vapor-liquid interface and the drag force, in terms of a sphere having the same volume as a bubble, there results

$$\frac{g}{g_o}(\rho_l - \rho_v)\frac{\pi D_s^3}{6} = \pi D_s \sigma_{lv} f_2(\beta) + C_D \frac{\pi D_s^2}{4}\frac{\rho_l u_b^2}{2g_o} \qquad (16)$$

At low heat-flux values single bubbles depart from single nucleating sites on the heating surface, the bubble velocity is small, and the drag force may be neglected. (From the data of Jakob (*7*) it may be shown that the numerical values of the buoyancy force and surface-tension force are nearly equal.) This case has been treated by Fritz (*5*) who obtained an expression relating the diameter of a bubble at the moment of breakaway from the heating surface and the angle of contact:

$$\frac{D_s}{\left[\dfrac{g_o\sigma_{lv}}{g(\rho_l - \rho_v)}\right]^{1/2}} = C_4\beta \qquad (17)$$

The dimensionless form of Equation (17) is due to the functional relationship in Equation (16). To determine the relationship analytically would require specification of the bubble geometry. The experimental data employed in obtaining the correlation were for bubbles of hydrogen and bubbles of steam at low heat fluxes. To indicate that Equation (17) will not correlate data at intermediate or high heat fluxes the data obtained in this investigation are illustrated in Figure 4. The line of Fritz is shown for comparison.

At high heat-flux values large bubbles grow from vapor patches on the heating surface, and the bubble velocities are such that the surface-tension force may be neglected. (From the data of this work it may be shown that the buoyancy force is greater than the surface-tension force by an order of magnitude.) The resulting equation is used to define the drag coefficient. The experimental data are replotted in Figure 5 as drag coefficient vs. Reynolds number. The solid lines represent the usual drag coefficient-Reynolds number curves for solid bodies falling through a liquid medium with sphericity as a parameter. The dashed line represents an extension of the $\psi = 0.94$ line through the experimentally determined points. An ellipsoid having the ratio $a:b:c = 2:1:1$ yields a sphericity of 0.93. The triangles represent the data obtained at breakoff ($\psi = 0.94$ to 1.00). It is of interest to note that all of the points fall in the region, for flow past a solid object, characterized by a transition from laminar to turbulent flow in the boundary layer resulting in a shift of the separation point.

At intermediate heat-flux values the bubble velocity is such that the drag and surface-tension force are of the same order of magnitude. Rearranging Equation (16) one finds the following dimensionless groups:

$$\frac{D_s}{\left[\dfrac{g_o\sigma_{lv}}{g(\rho_l - \rho_v)}\right]^{1/2}}, \frac{gg_o\sigma_{lv}}{u_b^4(\rho_l - \rho_v)}, \frac{\rho_l - \rho_v}{\rho_l}, f_2(\beta) \qquad (18)$$

where the drag coefficient has been assumed constant and the exponent on the group containing the velocity term has been omitted. In order to use Equation (16) in dimensionless form it is necessary to specify the bubble geometry such that $f_2(\beta)$ is known. Rather than do this it is assumed that $f_2(\beta)$ is proportional to β and that the dimensionless groups can be related to each other by an equation of the form

$$\frac{D_s}{\beta\left[\dfrac{g_o\sigma_{lv}}{g(\rho_l - \rho_v)}\right]^{1/2}} = C_5\left[\frac{gg_o\sigma_{lv}}{u_b^4(\rho_l - \rho_v)}\right]^{n_2} \qquad (19)$$

where the group $(\rho_l - \rho_v)/\rho_l$ will under most conditions have a value of unity. The data are plotted in Figure 6 and the value of n_2 determined as -0.22 and C_5 as 0.4. Figure 7 replots on rectangular coordinates. One point ob-

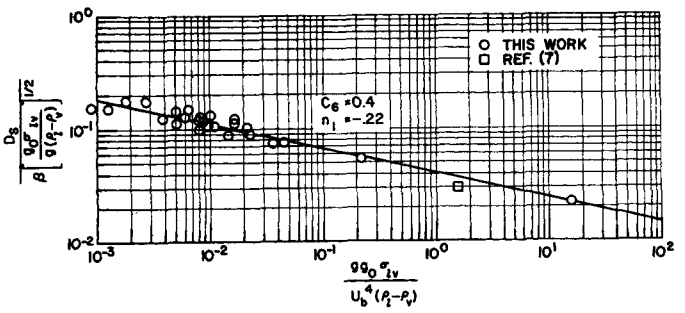

Fig. 6. Graphical determination of constants for Equation (24).

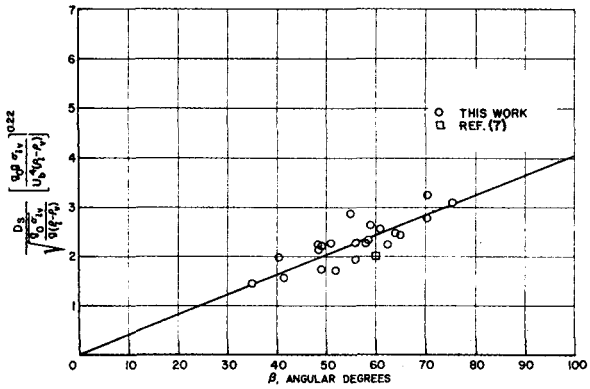

Fig. 7. Correlation of contact angle, bubble velocity, and bubble diameter at breakoff.

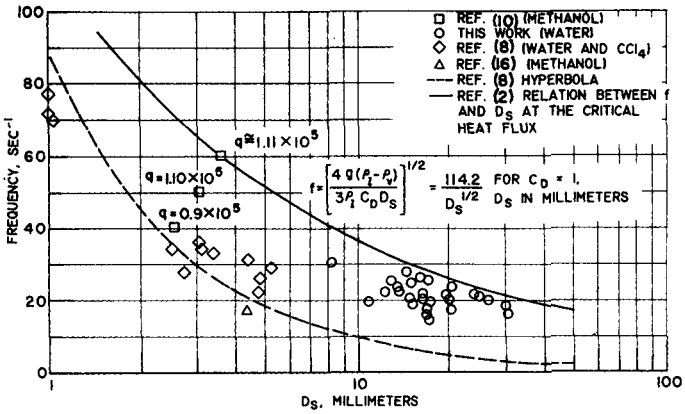

Fig. 8. Frequency of bubble formation vs. bubble diameter at breakoff.

tained from the literature, at a low heat flux, is included.

Bubble frequency

Jakob (*8*), generating vapor bubbles of steam and carbon tetrachloride at low heat fluxes, found the product of the bubble diameter at breakoff and the frequency of bubble formation to be approximately constant, as represented by the hyperbola (dashed line) in Figure 8. Perkins and Westwater (*10*), generating vapor bubbles of methanol over the entire boiling range, verified Jakobs results up to 80% of the critical heat flux. The value obtained over this wide range is indicated by the point marked $q = 0.9 \times 10^5$ in Figure 8. Between 80% of the critical heat flux, and the critical heat flux, both the frequency of bubble formation and the bubble diameter at breakoff were found to increase. Two points determined from their curves are labeled $q = 1.1 \times 10^5$ and $q = 1.11 \times 10^5$. The critical heat flux was found to be 1.15×10^5 (B.t.u.)/(hr.)(sq. ft.). Also included is an average value reported by Westwater and Santangelo (*16*) for methanol, corresponding to a heat flux of 0.945×10^5 (B.t.u.)/(hr.)(sq. ft.). The data for water in the neighborhood of the critical heat flux, as obtained in this work, is seen to yield a much higher bubble diameter at breakoff than that obtained for methanol in the region of the critical heat flux; it also yields a lower frequency of formation.

Freely rising vapor bubbles

The nontriangular points in Figure 5 represent data obtained on vapor bubbles rising freely through the liquid medium. It was found that all of the bubbles investigated fell in the Reynolds number range 1,000 to 100,000, where the drag coefficient is essentially independent of Reynolds number. The number of nontriangular points in Figure 5, for each sphericity, is not indicative of the shape (sphericity) distribution for the bubbles investigated. In fact the major portion of the freely rising bubbles were nonspherical in shape and were calculated to have a sphericity in the range 0.93 to 0.95. Only five points are shown as the overall Reynolds number range was only 20,000 to 50,000. It is thus of interest to note that vapor bubbles, rising freely for a short distance above the heating surface, can be represented by the usual drag coefficient-Reynolds number curves for solid bodies and in addition that at high heat fluxes the major portion of the bubbles investigated were nonspherical, had a sphericity range of 0.93 to 0.95, and a drag coefficient in the immediate neighborhood of unity. It has been observed by other investigators (*15*) that the motion of gas or vapor bubbles rising through a liquid medium may be erratic. Owing to the small distance between the ribbon and water surface in this work (3 in.) the observed bubble motion was fairly regular.

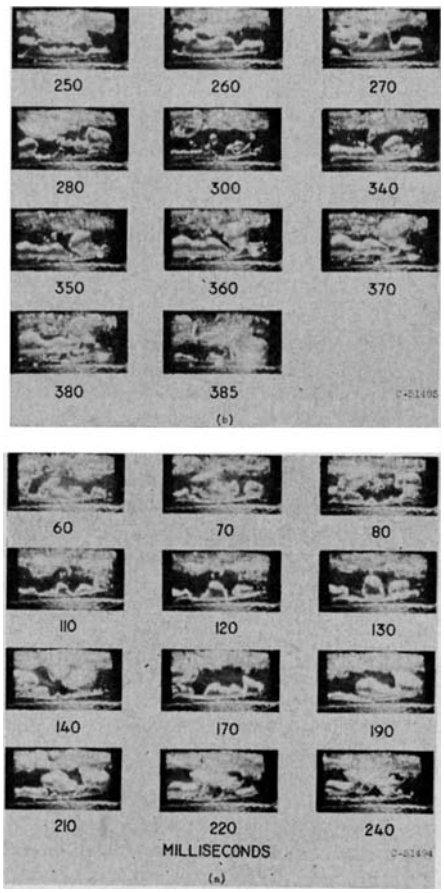

Fig. 9. Photographic study of boiling at the critical heat flux.

Deissler's analysis

The basic assumption of Deissler's analysis (*2*) is that the critical heat flux occurs when successive bubbles leaving the surface touch and coalesce. Under these conditions the product of the bubble frequency and the diameter at breakoff equals the rate at which the bubbles rise away from the surface:

$$f \cdot D_s = u_b \qquad (20)$$

Equating the buoyancy force to the drag force on a freely rising vapor bubble one obtains

$$\frac{g}{g_c}(\rho_l - \rho_v)\frac{\pi D_s^3}{6} = C_D \frac{\pi D_s^2}{4}\frac{\rho_l u_b^2}{2g_c} \qquad (21)$$

Solving for the velocity and rearranging

$$u_b = \left[\frac{4g(\rho_l - \rho_v)D_s}{3\rho_l C_D}\right]^{1/2} \qquad (22)$$

when one equates Equations (20) and (22) and solves for the frequency

$$f = \left[\frac{4g(\rho_l - \rho_v)}{3\rho_l C_D D_s}\right]^{1/2} \qquad (23)$$

When one utilizes the results of Figure 5 for freely rising vapor bubbles, C_D equals unity, the term $(\rho_l - \rho_v)/\rho_l$ is essentially unity, and the resulting expression is

$$f = \frac{114.2}{D_s^{1/2}} \qquad (24)$$

where D_s is in millimeters and the frequency in reciprocal seconds. Equation (23) is shown as the solid line in Figure 8. The agreement with experimentally determined frequencies and bubble diameters in the neighborhood

of the critical heat flux, from this work and reference (*10*), is reasonably good.

Pictures of the boiling action

Excerpts from the high-speed movies of the boiling action are shown in Figure 9. The pictures are from the final run in which simultaneously the power level was increased to a value well above the critical and the recording action begun. The film thus contains a record of the boiling action from just below the critical heat flux, through the transitional region, and to the burnout heat flux. Because the film must accelerate in the initial moments each frame is exposed for a longer period of time than when running at normal speed. As a consequence the frames during the first 60 msec. were overexposed, and although the bubble motion could be observed, because of the overexposure, none of those frames have been shown in Figure 9. Prior to increasing the power level the zirconium ribbon was under tension; thermal expansion however is evident in all of the frames after the power level is increased. The effectiveness of the glyptal coating in preventing boiling on the underface of the ribbon is also evident. At 340 msec. the ribbon is glowing noticeably at one end; at 370 msec. a glow is also apparent at the ribbon center, and it appears that this portion is becoming molten. At 385 msec. the intensity of the glow is increasing. For the next 25 msec. the frames were completely obliterated by the intensity of the glow and burnout occurred at the end of the ribbon although the center portion continued to glow for some time afterward. Upon removal of the ribbon from the water the center portion separated with only a slight touch.

One of the reasons for selecting zirconium as the ribbon material was the hope of obtaining some qualitative information on high temperature zirconium-water reactions, specifically at burnout. High-speed films obtained by Siegel and Usiskin (*13*) for burnout on a horizontal nichrome ribbon under both normal and zero gravity conditions show the ribbon glow prior to burnout but otherwise do not indicate any violence aside from the boiling action. In contrast burnout observed in this work, with a zirconium ribbon, appeared to be almost explosive in nature with the accompanying glow completely obliterating the individual frames. Owing to the relatively high chemical reactivity of zirconium it appears possible that a chemical reaction did occur.

SUMMARY

Frame-by-frame measurements were made of bubble diameters and bubble positions from high-speed photographs of the boiling phenomena. The data indicate that at high heat fluxes the primary forces acting on a bubble at breakoff are the buoyancy and drag forces. At high and intermediate heat fluxes the expression of Fritz (*5*) does not correctly predict the bubble diameter at breakoff. A dimensionless relationship is developed relating bubble velocities, bubble diameters, and contact angles. The relationship was determined from high heat-flux data obtained in this work, and one point at low heat flux was obtained from the literature (*7*).

It was found that for a short distance above the heating surface drag coefficients for freely rising vapor bubbles may be represented by the usual drag coefficient-Reynolds number curves for solid bodies. For conditions where the bubbles in general are not spherical, a drag coefficient of unity is reasonable.

Data was obtained with water to extend the relationship between bubble diameter at breakoff and the frequency of bubble formation at high heat fluxes. Previous data had been obtained by Perkins and Westwater (*10*) for methanol. A relationship proposed by Deissler (*2*), as a basis for his critical heat-flux correlation, was found to yield reasonable agreement with both fluids.

ACKNOWLEDGMENT

The author wishes to acknowledge the helpful advice and suggestions of Mr. Robert G. Deissler whose critical heat-flux analysis provided the incentive for this investigation.

NOTATION

a,b,c = semiaxes of an ellipsoid, ft.
C_i = constants, $i = 1,2,3,\ldots$
C_D = drag coefficient
D_s = diameter of a sphere having the same volume as a vapor bubble, ft. or mm. as specified
f = frequency of bubble formation, $(\text{sec.})^{-1}$
f_1 = functional relationship, Equation (9)
$f_2(\beta)$ = function of β, Equation (16)
g = acceleration of gravity, (ft.)/(hr.)^2
g_o = conversion factor, (lb.-mass)(ft.)/(lb.-force)(hr.)^2
K = defined by Equation (3)
m = constant
n_i = constants, $i = 1,2,3,\ldots$
N_{Nu} = Nusselt number
N_{Pr} = Prandtl number
N_{Re} = Reynolds number
N = defined by Equation (8)
q_c = critical heat flux, (B.t.u.)/(hr.)(sq. ft.)
S_b = surface area of an ellipsoid, (sq. ft.)
u_b = normal velocity of a vapor bubble, (ft.)/(sec.)
V_b = volume of an ellipsoid, (cu. ft.)

Greek Letters

β = contact angle, angular deg.
ϵ = eccentricity, $(a^2 - c^2)^{1/2}/a$
λ_v = latent heat of vaporization, (B.t.u.)/(lb.)
μ_l = liquid viscosity, (lb.)/(ft.)(hr.)
μ_v = vapor viscosity, (lb.)/(ft.)(hr.)
ρ_l = liquid density, (lb.)/(cu. ft.)
ρ_v = vapor density, (lb.)/(cu. ft.)
σ_{lv} = liquid-vapor surface tension, (lb.-force)/(ft.)
ψ = sphericity, defined by Equation (15)

Subscripts

b = bubble
c = critical
l = liquid
lv = liquid-vapor
s = sphere
v = vapor

LITERATURE CITED

1. Borishanskii, V. M., *Zhur. Tekh. Fiz.*, **26**, 452 (1956); Translated in *Soviet Physics—Technical Physics*, **1**, 438.
2. Deissler, R. G., Columbia University Heat Transfer Symposium, New York, New York (1954).
3. Forster, H. K., and N. Zuber, *J. Applied Phys.*, **25**, 474 (1954).
4. ———, *A.I.Ch.E. Journal*, **1**, 531 (1955).
5. Fritz, W., *Physik. Z.*, **36**, 379 (1935).
6. Griffith, Peter, *Trans. Am. Soc. Mech. Engrs.*, **80**, 721 (1958).
7. Jakob, Max, *Z. Ver. deut. Ing.*, **76**, 1161 (1932).
8. ———, "Heat Transfer," Vol. 1, pp. 66, 633, Wiley, New York (1949).
9. Kutateladze, S. S., *Izvest. Akad. Nauk S.S.S.R Otdel. Tekh. Nauk.*, **4**, 529 (1951).
10. Perkins, A. S., and J. W. Westwater, *A.I.Ch.E. Journal*, **2**, 471 (1956).
11. Plesset, M. S., and S. A. Zwick, *J. Appl. Phys.*, **25**, 493 (1954).
12. Rohsenow, Warren, and Peter Griffith, *Chem. Eng. Progr. Symposium Ser. No. 18*, **52**, 47 (1956).
13. Siegel, R., and C. Usiskin, presented at the Am. Soc. Mech. Engrs. Aviation Conference, Los Angeles, California, (March 9 to 12, 1959).
14. Sterman, L. S., *Zhur. Tekh. Fiz.*, **23**, 341 (1953).
15. Westwater, J. W., "Advances in Chemical Engineering," Vol. 1, pp. 20, 70, Academic Press, New York (1956).
16. ———, and J. G. Santangelo, *Ind. Eng. Chem.*, **47**, 1605 (1955).
17. Zuber, N., *Trans. Am. Soc. Mech. Engrs.*, **80**, 711 (1958).
18. ———, and M. Tribus, *AECU-3631* (1958).

Manuscript received October 5, 1959; revision received February 25, 1960; paper accepted February 29, 1960. Paper presented at A.I.Ch.E. Buffalo meeting.